ACS OMEGA

Open Access

http://pubs.acs.org/journal/acsodf

Article

Preparation and Characterization of Chlorin e6-Conjugated Au Nanoparticles as the Radiosensitizer for Enhanced Radiotherapy

Huanhuan Liu, Bing Xu, Lijuan Chen, Xiaochen Li, Huiqiang Li, Junting Liang, Yan Bai, and Meiyun Wang*

Cite This: *ACS Omega* 2026, 11, 439−448

Read Online

ACCESS | Metrics & More | Article Recommendations | Supporting Information

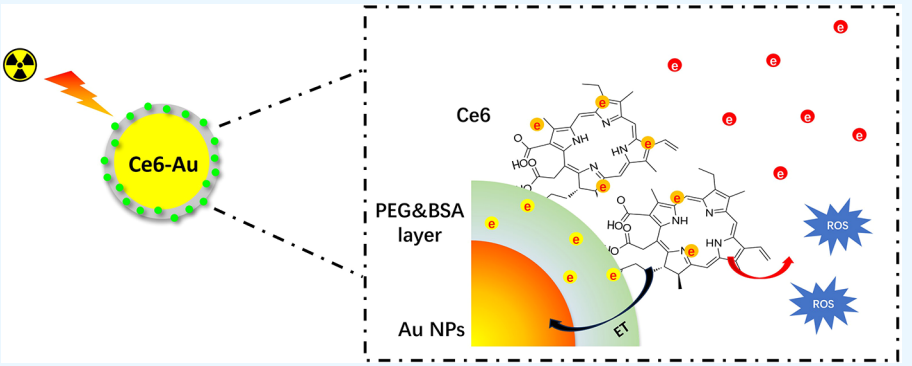

ABSTRACT: The interaction between ionizing radiation and materials composed of high Z-number elements could be applied to enhance radiotherapy. In this work, we fabricated an ionizing radiation-sensitive nanoplatform by grafting chlorin e6 (Ce6) onto the surface of ultrasmall gold nanoparticles (Au NPs), aiming to enhance the radiation effects induced by different radiation sources. Poly(ethylene glycol) (PEG) was applied as the shape-controlling agent during the synthesis of Au nanoparticles. The as-prepared Au NPs show excellent monodispersity, with an average hydrodynamic diameter of around 5 nm. U87 and HeLa cell lines were utilized to evaluate the biological properties of the as-prepared Ce6−Au NPs. The Cell Counting Kit-8 (CCK-8) results reveal that the Ce6−Au NPs conjugate can significantly affect the growth of U87 cells under X-ray and ^{68}Ga exposure, which is not seen for the pure Au NPs, Ce6, and physically mixed Ce6 and Au NPs. Moreover, the Ce6−Au NPs conjugate show evident cell prefoliation inhibition of U87 and HeLa cells under both X-ray and ^{18}F-radiolabeled fluorodeoxyglucose (^{18}F-FDG) exposure. These results indicate that interaction exists between Ce6 and Au NPs under radiation exposure. The mRNA sequencing results show that the tumor killing performance induced by Ce6−Au NPs may be due to regulation of the tumor microenvironment (TME) and immune-relevant signaling pathway. Our research proves that the rational combination of Au NPs and Ce6 can make better use of ionizing radiation energy and thus improve the therapeutic outcome of radiotherapy.

1. INTRODUCTION

Radiotherapy is one of the main approaches for cancer treatment. The underlying mechanism is that tumor cells are more sensitive to ionizing radiation than healthy tissues and thus more effect is needed to repair the radiation-induced DNA damage.[1] Regarding the fact that human tissues are mainly composed of light elements such as C, H, and O, the majority of ionizing radiation power just passes through the human body. Therefore, it usually requires a high radiation dose to inhibit the tumor progress, which no doubt will pose unexpected radiation damage to healthy tissues. High Z-number elements, such as Au and Hf, have large stopping power and can deposit more radiation energy, which could be applied in radiotherapy for enhanced therapeutic effects.[2] Au nanoparticles have been studied as radiosensitizers for years, and the influencing factors such as size, shape, and surface modification on Au-enhanced radiotherapy have been comprehensively studied.[3,4] Though Au particles with large sizes, in theory, can absorb more radiation power, ultrasmall gold nanoparticles are preferred due to the diverse modification possibility and kidney excretion which hinder the long-term toxicity of nanoparticles.[5]

The Au nanoparticles can interact with ionizing radiation, the primary energy migration between the highly energetic photons and radiosensitizer will induce physical enhancement, and in this way produce electrons such as secondary electrons (~10^2−10^5eV), intermediate energy (~0.1−100 eV), and thermalized

Received: May 25, 2025
Revised: December 9, 2025
Accepted: December 12, 2025
Published: December 23, 2025

Scheme 1. Illustration of the Fabrication of the Ce6−Au Nanoparticle Complex and Its Therapeutic Mechanism under Ionizing Radiation Exposure

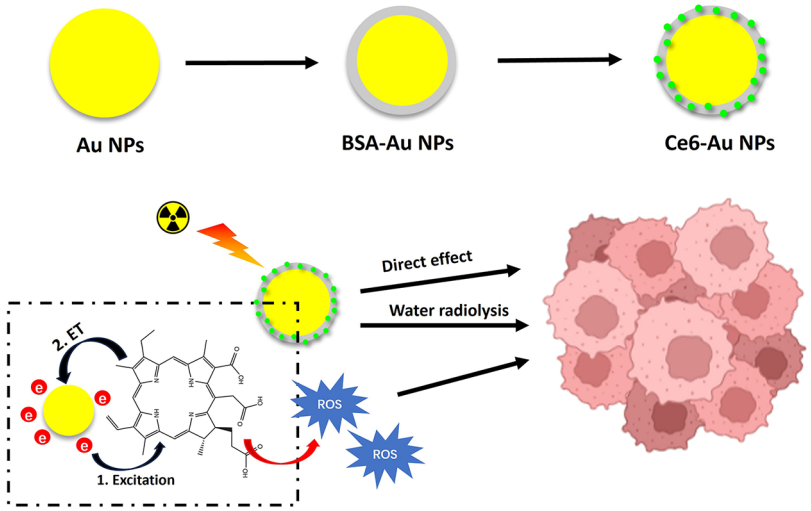

excitations (<0.1 eV).[6,7] The as-produced electrons with higher energy have a micrometer-level range in water, while the low-energetic ones can only pass through a few nanometers. To make full use of these electrons, gold-based heterostructures have been fabricated.[8] For instance, Wang developed a hybrid nanoplatform based on Au−Bi_2S_3 nanoparticles which have a typical Schottky-type heterostructure for enhanced radiotherapy.[9] Apart from capturing more X-ray energy at tumor sites, the presence of Bi_2S_3 can also make use of the low-energy electrons to produce nonoxygen-dependent free radicals. Besides, the Schottky-type barrier can transfer X-ray-generated electrons and achieve better electron−hole pair separation. Nevertheless, Cheng also developed a gold-based nanoscaled heterostructure composed of Au and TiO_2 for enhanced radiotherapy.[10] The hybrid anisotropic nanostructure not only makes use of more X-ray-induced low-energy electrons but also causes better separation and migration of electron−hole pairs, which can generate more ROS and thus affect the tumor growth.

Chlorin e6 (Ce6) is a commonly used photosensitizer in photodynamic therapy. Upon light irradiation, it generates singlet oxygen ($^1O_2$), which is lethal to tumor cells. However, its limited light utilization efficiency restricts its broader therapeutic application. Studies have shown that conjugating Ce6 with functional nanoparticles can effectively improve the photon absorption and energy conversion of Ce6 molecules.[11] The plasmon resonance energy transfer from gold can increase the amount of $^1O_2$ produced by light-irradiated Ce6, thus many Ce6−Au conjugates have been explored for enhanced photodynamic therapy.[12] In addition, our previous study revealed that Ce6 can also response to ionizing radiation exposure,[13] which is not surprising since its analogue PpIX is a widely studied radiosensitizer.[14] Moreover, Kamkaew et al. proved that the radioisotope ^{89}Zr can also excite Chlore 6 and produce ROS for killing tumors.[15]

Herein, we fabricated a gold nanoparticle−Ce6 complex for enhanced radiotherapy and briefly studied its antitumor mechanism. The PEG-coated ultrasmall gold nanoparticles were first synthesized and further decorated with BSA to enhance their biocompatibility. Ce6 was chemically grafted onto the gold nanoparticle to form a heterostructure for more utilization of the ionizing radiation. X-rays, ^{18}F-FDG, and ^{68}Ga-DOTATATE were all applied as radiation sources for activating the antitumor effects of Ce6−Au NPs. Two cell lines, U87 and HeLa, were used to test the radiation enhancement of the Ce6−Au NPs. Additionally, the mechanism for enhanced radiotherapy in the presence of radiosensitizers was studied by varying the approaches to drug administration and radiation protocols. Moreover, the therapeutic mechanism of Ce6−Au NPs was also studied by mRNA transcriptome sequencing (Scheme 1).

2. EXPERIMENTAL SECTION

2.1. Materials. Gold chloride trihydrate (≥99.9%, $HAuCl_4 \cdot 3H_2O$), 1-(3-(dimethylamino)propyl)-3-ethylcarbodiimide hydrochloride (EDC), *N*-hydroxy succinimide (NHS), bovine serum albumin, and phosphate-buffered saline (PBS) standard buffer powder were purchased from Macklin (Shanghai, China); sodium borohydride ($NaBH_4$) was purchased from Kermel Co., Ltd. (Tianjin, China); PEG-SH (Mw = 750/1000 Da) was obtained from Tanshtech Co., Ltd. (Guangzhou, China); chlorin e6 (Ce6) was purchased from Yuanye Bio-Technology Co., Ltd. (Shanghai, China). Dulbecco's modified Eagle's medium (DMEM) and Cell Counting Kit-8 (CCK-8) were purchased from Servicebio Technology Co., Ltd. (Wuhan, China). Fetal bovine serum (FBS) was purchased from Thermo Scientific. ^{18}F-FDG and ^{68}Ga-DOTATATE were obtained via the routine nuclear imaging medicine synthesis process in Henan Provincial People's Hospital.

2.2. Synthesis. *2.2.1. Synthesis of Au-PEG NPs.* The monodispersed Au NPs were synthesized via a simple $NaBH_4$ reduction approach. Typically, 150 μL of $HAuCl_4$ aqueous solution (0.1 M) was mixed with 5 mL of PEG-SH (2.4 mM, MW = 750 or 1000 Da) and stirred for 20 min at room temperature. Then, 1 mL of $NaBH_4$ (0.05 M) was poured to the Au precursor solution. The yellowish solution immediately turned purple-red. The mixture was stirred for another 20 min and then filtered by a 220 nm syringe filter to remove large aggregates; the obtained purple-red solution was collected and kept at 4 °C for storage.

2.2.2. Synthesis of BSA-Coated Au NPs. Bovine serum albumin (BSA) was used for the surface modification of Au NPs. Simply, BSA solution (0.5 mL, 2 mg/mL) was mixed with 4 mL of PEG-Au NPs solution overnight, and the mixture was then

https://doi.org/10.1021/acsomega.5c04914
ACS Omega 2026, 11, 439−448

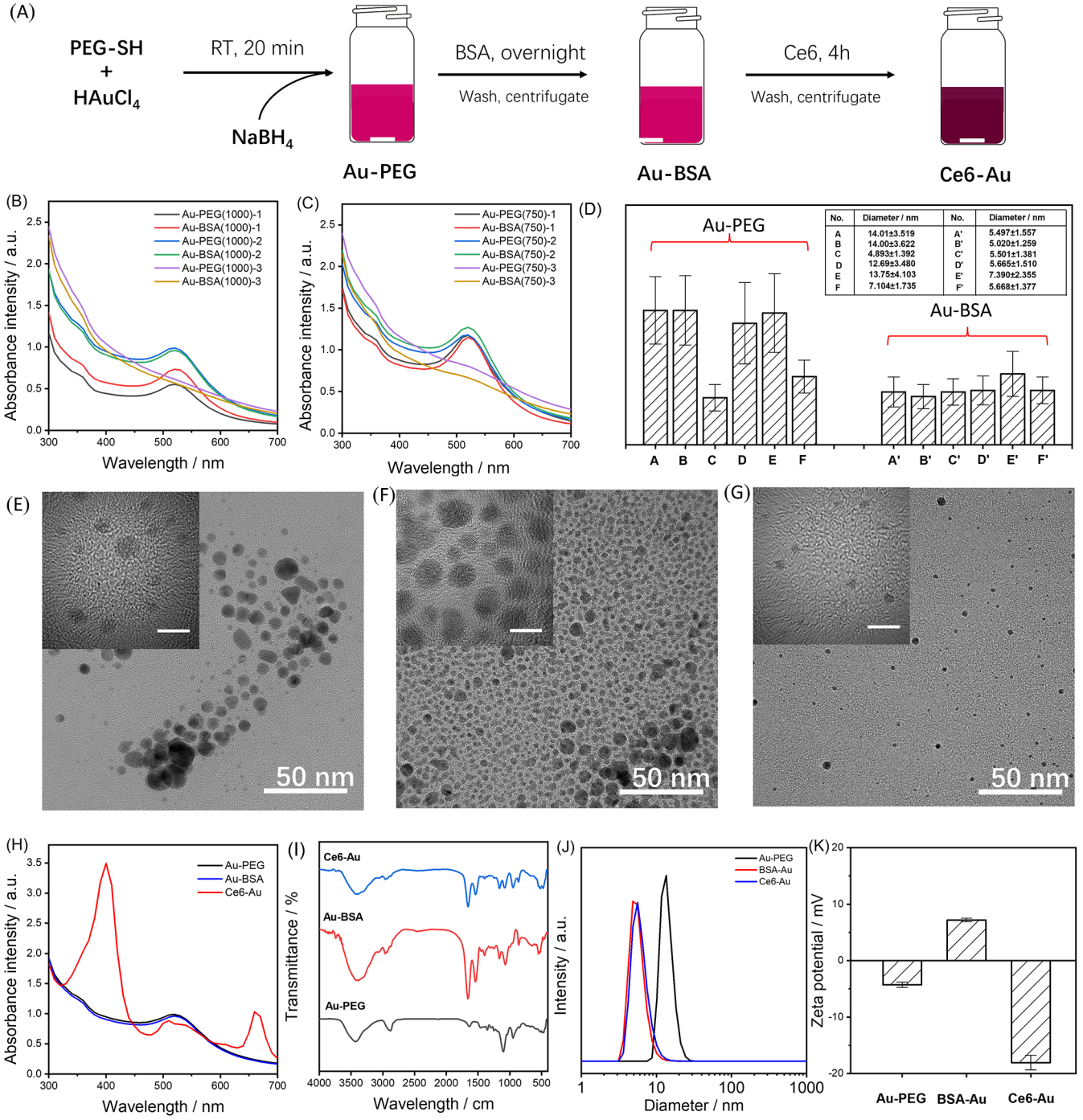

Figure 1. (A) Synthesis procedure of Au−Ce6 NPs. UV−vis spectra of Au NPs prepared in the presence of (B) PEG-1000 and (C) PEG-750 (Au-PEG(1000)-1: molar ratio between PEG-1000 and the Au precursor is 0.08; Au-BSA(1000)-1: BSA-modified Au-PEG(1000)-1; Au-PEG(1000)-2: molar ratio between PEG-1000 and the Au precursor is 0.32; Au-PEG(1000)-3: molar ratio between PEG-1000 and the Au precursor is 0.8; the same terminologies apply to PEG-750 samples). (D) Hydrodynamic diameter of different Au NPs (A: Au-PEG(1000)-1; B: Au-PEG(1000)-2; C: Au-PEG(1000)-3; D: Au-PEG(750)-1; E: Au-PEG(750)-2; F: Au-PEG(750)-3; A': Au-BSA(1000)-1; B': Au-BSA(1000)-2; C': Au-BSA(1000)-3; D': Au-BSA(750)-1; E': Au-BSA(750)-2; F': Au-BSA(750)-3). TEM images of the obtained (E) Au-PEG(1000)-1, (F) Au-PEG(1000)-2, and (G) Au-PEG(1000)-3 (the bar in the inner figure is 5 nm). (H) UV−vis spectra, (I) FT-IR spectra, (J) size distribution, and (K) ζ-potential of the obtained Au samples (Au-PEG: Au-PEG(1000)-2; Au-BSA: Au-BSA(1000)-2; Ce6−Au: Ce6-grafted Au NPs).

collected with centrifugation filter tubes (100 kDa, 4000 rpm, 30 min).

2.2.3. Synthesis of Ce6-Loaded Au NPs. 6 mg of 1-(3-(dimethylamino)propyl)-3-ethylcarbodiimide hydrochloride (EDC), 6 mg of *N*-hydroxy succinimide (NHS), and 4 mg of Ce6 were dispersed in 2 mL of DMSO and stirred overnight in the dark. 100 μL of activated Ce6 solution was added to 2 mL of BSA-coated Au NPs and stirred overnight. The resultant product was then collected with centrifugation filter tubes and washed twice with PBS.

2.3. Characterization. The shape and size of the Au-PEG NPs were imaged with a 120 kV JEM-1400 Plus transmission

https://doi.org/10.1021/acsomega.5c04914
ACS Omega 2026, 11, 439−448

electron microscope (JEOL JEM-2100F). The absorption spectrum of the obtained samples was measured using an ELISA reader (BioTek) coupled with a UV−vis detector. The hydrodynamic diameter and ζ-potential of the Au-PEG NPs were determined with a zeta sizer (Nano-ZS, Malvern). The surface functional groups of the obtained samples were recorded using a Fourier transform infrared (FT-IR) spectrometer (Shimadzu-IRTracer 100, Japan). An ICP−MS facility was utilized to quantify the number of metal ions.

2.4. Cell Culture. U87 human glioblastoma cells and HeLa cells were cultured in DMEM supplemented with 10% FBS under a humidified atmosphere containing 5% CO_2 at 37 °C.

2.5. Cell Uptake and Cellular Distribution. Confocal microscopy (LSM 980, ZEISS) was used to determine the cellular uptake of Ce6−Au NPs in U87 and HeLa cells. The cells (1×10^4) were seeded in an 8-well chamber coverslip (ibidi) and cultured overnight. 20 μL of Ce6−Au NPs solution was added and incubated for 12 h. The cells were washed three times with PBS and fixed with 4% paraformaldehyde solution for 15 min. After fixation, the cells were washed three times with PBS and stored in a refrigerator. Prior to imaging, Hoechst 33342 (Thermo Fisher Scientific) was prepared according to the product protocol and added to the cells. Laser excitation was performed at 405 nm, with emission detected at 465 nm for Hoechst 33342 and at 660 nm for Ce6. The acquired data were analyzed by using ImageJ software.

To evaluate the cell uptake, 1×10^6 cells were seeded in a 10 cm plate. After 16 h, Au solution with different samples was fed to each vial and waited for 12 h for the cell to uptake. Then, the suspension was removed, the cells were washed with PBS three times, the cells were detached with 1.5 mL trypsin for 5 min, and after adding 2.5 mL of culture medium to the vial to neutralize the detaching process, this solution was collected and the cell number was measured. To measure the Au concentration, the cell solution was centrifuged at 4000 rpm for 10 min and the top solution was removed, then 1 mL of aqua regia was added to dissolve the cells and gold, and after being sonicated for 60 min at 45 °C, 19 mL of MQ was added to the system. Finally, the sample was transferred into the ICP equipment (ICP−MS, Agilent 7850) for measuring the Au concentration.

2.6. Cell Viability Tests. U87/HeLa cells were plated on 96-well plates with a cell density of 3000 cells/well (100 μL/well) and incubated overnight. Then, 10 μL diluted samples were added to each well and incubated for another 18 h, which was followed by irradiation with a 320 keV X-ray source (PXI X-RAD 320, Precision X-ray Inc.) at doses of 2 Gy, 4 Gy, 6 Gy, and 8 Gy. After 24 h, the CCK-8 assay was carried out to evaluate the cell viability. The absorbance of cells at 450 nm was measured by an ELISA reader (PowerWave XSTM, Bio-Tek) after incubation of cells. The cells treated with PBS were recognized as the control group.

The viability of the cells treated with Au NPs and ^{18}F-FDG/^{68}Ga-DOTATATE were carried out in a similar approach. 0 kBq, 50 kBq, 100 kBq, 200 kBq, and 500 kBq units of ^{18}F-FDG/^{68}Ga-DOTATATE were given to the cells as internal radiation sources. The CCK-8 assay was conducted 24 h later.

2.7. Colonial Assay. U87 cells were plated on 6-well plates with a cell density of 3000 cells/well (2.5 mL/well) and kept overnight. Then, 250 μL diluted samples were added to each well and incubated for another 18 h, which was followed by irradiation with a 320 keV X-ray source (PXI X-RAD 320, Precision X-ray, Inc.) at a dose of 2 Gy or adding 200 kBq of ^{18}F-FDG. After being further incubated for 2 weeks, the cells were washed with PBS, and the cells were fixed with paraformaldehyde (4 °C, 60 min), which was followed by being stained with crystal violet staining solution (0.5%, Kemiou Chemical Reagent). The colonial assay of HeLa cells was carried out with the same protocol, but the X-ray radiation dose was increased to 6 Gy and the incubation time was shortened to 10 days.

2.8. mRNA Transcriptome Sequencing. Sample preparation: 1×10^5 U87 cells were seeded in a 6-well plate with 2 mL of culture medium and incubated at 37 °C overnight, followed by the addition of 200 μL of PBS buffer and Au−Ce6 sample to each well. After incubating for another 24 h, the cells were exposed to 4 Gy X-ray radiation. Culture medium was removed 48 h after X-ray exposure, and 1 mL of TRIzol reagent was added to each well for extracting mRNA. The cells were collected until all of them dissolved, and the samples were frozen in liquid nitrogen and stored at −80 °C. The samples were sent to GENEWIZ Biotechnology Co., Ltd. (Suzhou, China) for sequencing analysis.

2.9. Statistical Analysis. Data are presented as mean ± standard deviation based on at least five independent replicates. Student's t test or one-way analysis of variance (ANOVA) was applied for comparison among the obtained results. p values: ns, $p > 0.05$; *$p \leq 0.05$; **$p \leq 0.01$; ***$p \leq 0.001$.

3. RESULTS AND DISCUSSION

PEG-decorated Au nanoparticles were first synthesized via a simple reduction method with $NaBH_4$, and thiol-PEG was applied as the stabilizing agent. BSA was applied to further modify the surface of Au nanoparticles. The widely used photosensitizer chlorine e6 (Ce6) was chemically grafted to the surface of the Au-BSA nanoparticles via the interaction between the COOH group of Ce6 and the NH_2 group of BSA (Figure 1A). PEG polymers with different chain lengths were utilized to form ultrasmall nanoparticles with excellent dispersibility in aqueous systems. Three molar ratios (PEG:Au precursor) were chosen, say 0.08, 0.32, and 0.8, to study the influence of the molar ratio on the synthesis of Au nanoparticles. The UV−vis spectra of the obtained samples are shown in Figure 1B,C; an evident peak at 520 nm could be observed for Au-PEG(1000)-1 and Au-PEG(1000)-2 samples, which correspond to the surface plasmon peaks of Au NPs.[16] However, this peak disappears for the Au-PEG(1000)-3 sample with the largest PEG:Au molar ratio; this phenomenon could also be observed for PEG-750-coated Au NPs. According to previous publications, the morphology and surface engineering can affect the UV−vis absorption spectrum of Au NPs,[17,18] and the exact reason for the peak disappearance needs to be further studied by other characterization methods.

DLS analysis was performed to record the size distribution of the as-prepared Au NPs (Figure S1). As illustrated in Figure 1D, samples Au-PEG(1000)-1 and Au-PEG(1000)-2 show a mean hydrodynamic diameter of around 14 nm, while for Au-PEG(1000)-3 it is around 5 nm. After BSA coating, the hydrodynamic diameters for the three samples change to ∼5 nm. The results also reveal that the surface of Au-PEG NPs is not entirely covered when using relatively less PEG polymers.[19] Similarly, this phenomenon could also be seen for Au-PEG NPs prepared with PEG-750. The TEM images of the Au-PEG(1000)-1 sample formed with fewer PEG polymers show a complex microstructure, and apart from the spherical structure, we can also notice triangle- and rod-shaped nanoparticles (Figure 1E). In contrast, the Au-PEG(1000)-2 sample

https://doi.org/10.1021/acsomega.5c04914
ACS Omega 2026, 11, 439−448

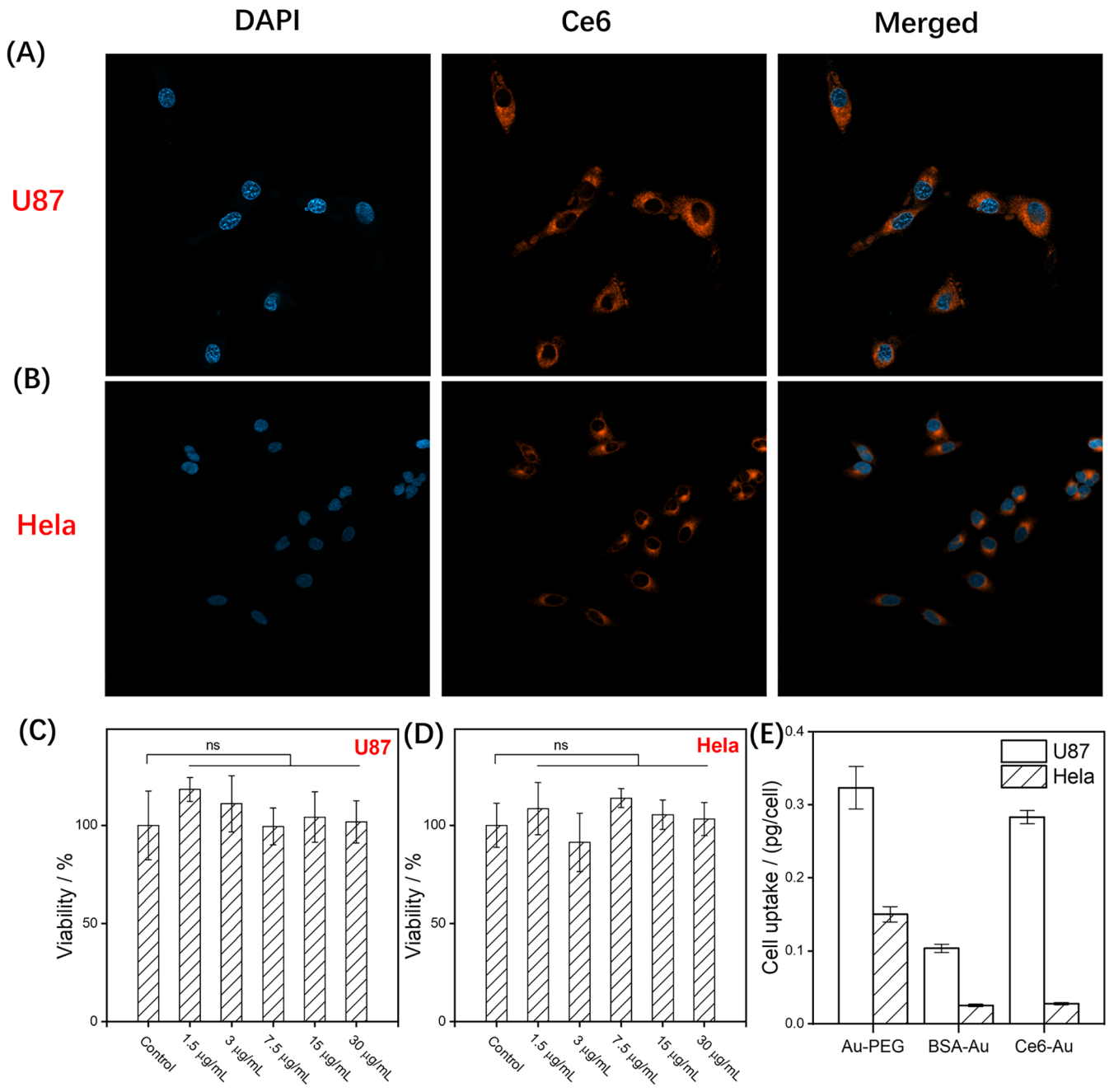

Figure 2. Intracellular distribution of Ce6−Au in (A) U87 cells and (B) HeLa cells imaged by the confocal laser scanning microscopy after being incubated for 12 h. Evaluation of the biotoxicity of the Au-PEG nanoparticles with the (C) U87 cell line and (D) HeLa cell line ($n = 5$). (E) Cell uptake of the Au-PEG nanoparticles in U87 and HeLa cell lines ((n = 3), the final concentration of Au in each sample is 18 μg/mL, and the final Ce6 concentration is 3.6 μg/mL).

is composed of spherical nanoparticles, the majority of which are around 5 nm (Figure 1F). Additionally, the Au-PEG(1000)-3 sample is composed of ultrasmall particles around 2 nm (Figure 1G). The TEM results prove that the PEG polymers act as shape-control agents during the synthesis of Au NPs.

Au-BSA(1000)-2 was used for further modification. According to our previous work, the widely used photosensitizer Ce6 can somehow respond to high-energy X-rays and γ-rays.[13] So, we aimed to use it as a radiation sensitizer to further enhance the response of Au NPs to ionizing radiation. Ce6 was attached to Au-BSA NPs via the EDC/NHS method.[20] The UV−vis absorption spectrum is shown in Figure 1H, and we can see the typical absorbance of Ce6, evidenced by the Soret band at 400 nm and the Q-band at 660 nm. In the FT-IR spectrum shown in Figure 1I, the bands at 1063 and 1103 cm^{-1} correspond to the C−O stretching vibrations which are representative of PEG. After being modified with BSA, two bands appear at 1655 and 1540 cm^{-1}, which correspond to the amide I and amide II of protein. The addition of Ce6 does not induce any change.[16] The introduction of BSA and Ce6 into these Au-PEG nanoparticles can influence their surficial properties. As shown in Figure 1J,K, though the modification of Ce6 does not influence the hydrodynamic radius of BSA-Au NPs, the ζ-potential changed to −18 mV from 7 mV.

After successfully preparing the Au nanoparticles, we first determined the intracellular distribution of Au−Ce6 in U87 and

https://doi.org/10.1021/acsomega.5c04914
ACS Omega 2026, 11, 439−448

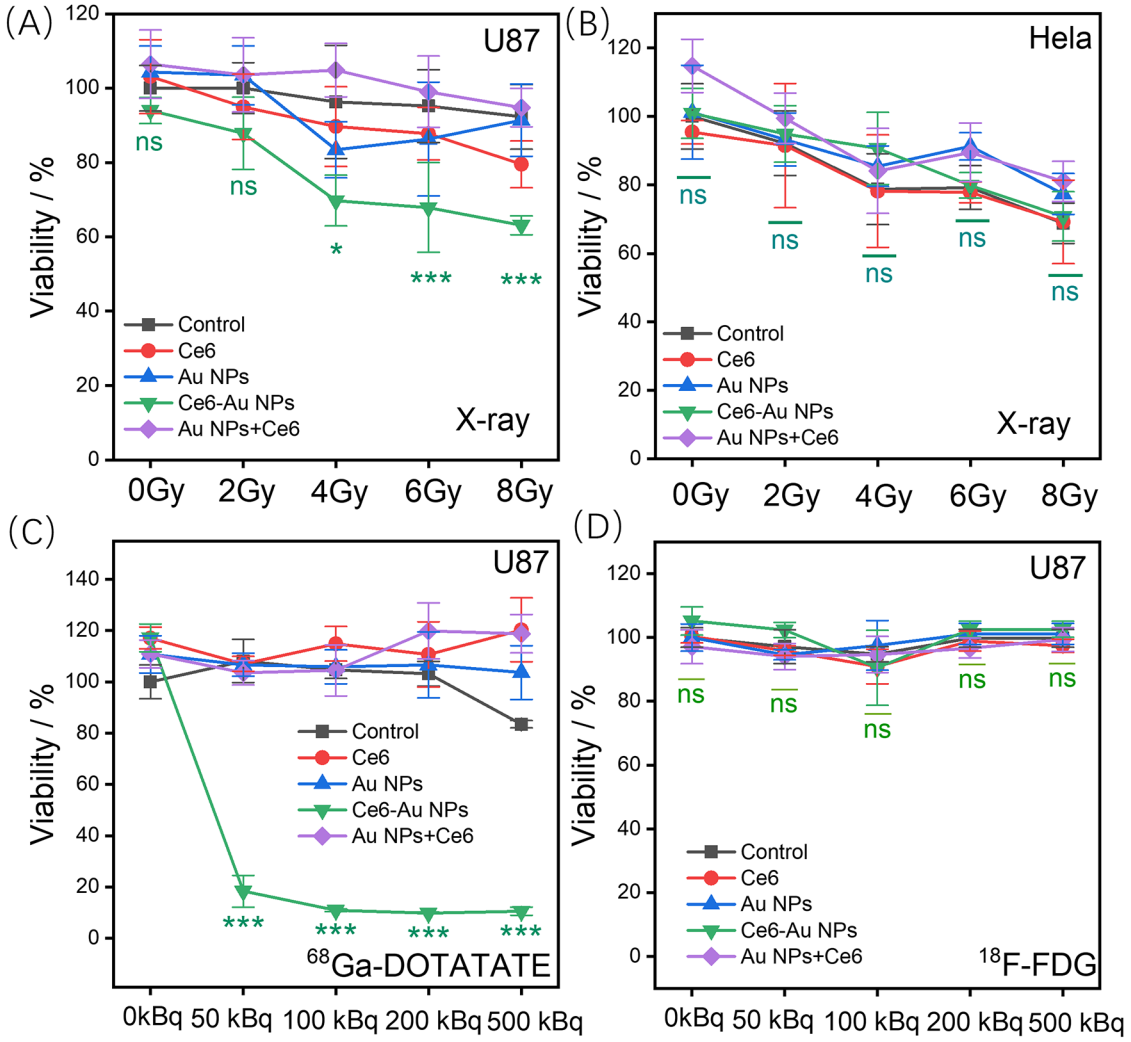

Figure 3. Cell toxicity of the as-prepared samples on (A) U87 and B (HeLa) cell lines under X-ray exposure. Cell toxicity of the as-prepared samples on the U87 cell line under (C) ^{68}Ga-DOTATATE exposure and (D)^{18}F-FDG exposure. Ce6: Ce6 concentration is 3.6 μg/mL; Au NPs: Au concentration is 18 μg/mL; Ce6−Au NPs: Ce6 concentration is 3.6 μg/mL and the Au concentration is 18 μg/mL; Au NPs+Ce6: Ce6 and Au are physically mixed together, and the concentrations of Ce6 and Au NPs are 3.6 and 18 μg/mL, respectively.

HeLa cells by confocal laser scanning microscopy (CLSM). The nuclei were stained with Hoechst 33342 which show blue fluorescence after being excited by a 405 nm laser light, while Ce6 shows red fluorescence under the same excitation light. As shown in Figure 2A,B, after being incubated for 12 h, Ce6−Au could successfully penetrate through the cell membrane of U87 and HeLa cells and accumulate at the lysosomes. Next, we evaluated the biocompatibility of the Au-PEG nanoparticles. The as-prepared Au-PEG samples were fed to the U87 cells and HeLa cells, resulting in final concentrations of 1.5 μg/mL to 30 μg/mL. As shown in Figure 2C,D, comparable cell viability has been observed with different Au concentrations, which indicates that Au nanoparticles have negligible cell toxicity under experimental conditions. The consequent cell uptake experiment reveals that the U87 cells in general have a higher uptake of Au NPs than HeLa cells. The cell uptake of U87 cells for Au-PEG is 0.323 ± 0.029 pg/cells, which is higher than that of BSA-Au and Ce6−Au, with cell uptake of 0.104 ± 0.006 pg/cells and 0.283 ± 0.009 pg/cells, respectively.

Cell killing performance of different Au nanoparticles in radiotherapy was determined by the CCK-8 assay. We seeded U87 cells and HeLa cells in 96-well plates, then administered different samples to these cells, and then irradiated them with different radiation sources. As shown in Figure 3A, U87 cells treated with both Ce6 and Au nanoparticles did not show evident difference than the control group, even at 8 Gy dose. By contrast, the cells that were fed with Ce6−Au nanoparticles exhibit noticeably lower viability, showing only 63.14 ± 2.54% of U87 cells stayed alive compared to the control group with 92.29 ± 8.68% cells being kept alive after receiving 8 Gy of X-ray radiation. One interesting phenomenon is that the cells that were treated with physically mixed Ce6 and Au NPs do not show evident cell growth inhibition. By comparison, HeLa cells, which in theory are more sensitive to ionizing radiation, do not show any noticeable difference after being treated with different samples compared with the control group (Figure 3B), which may be related to the less uptake of radioenhancers. Considering the fact that it may take a longer time to observe the radiation damage, the colony formation assay was also carried out to explore the influence of Au NPs and Ce6−Au on the proliferation of X-ray-irradiated U87 cells. The results in Figures S4 and S5 indicate that addition of Au NPs can evidently influence the colony formation of U87 cells and HeLa cells after being exposed to X-ray radiation. The Ce6−Au samples can

https://doi.org/10.1021/acsomega.5c04914
ACS Omega 2026, 11, 439−448

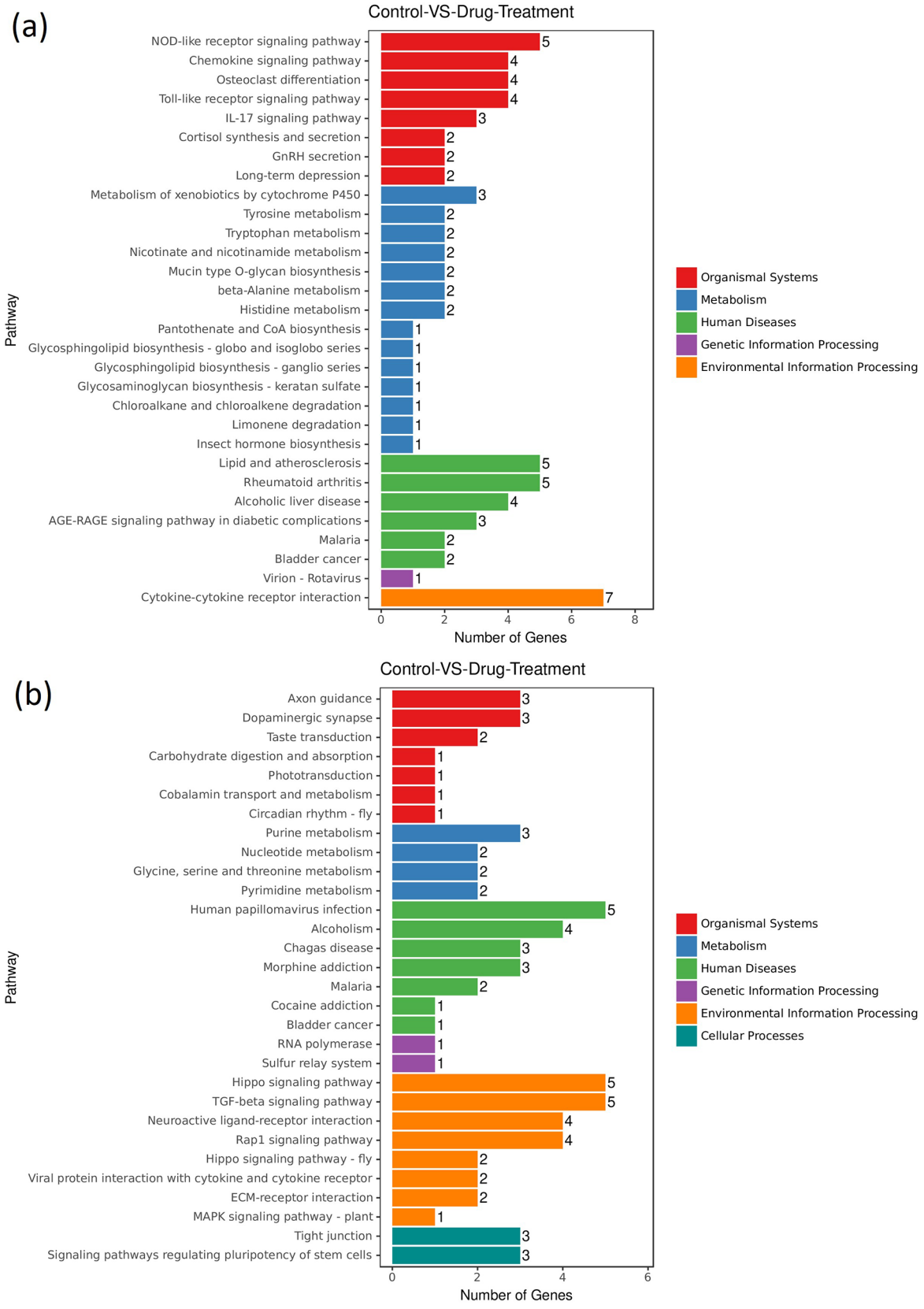

Figure 4. KEGG pathway analysis of the difference between the Ce6−Au+X-ray (6 Gy) treatment group and X-ray (6 Gy) treatment group. (A) Pathway enrichment analysis of upregulated genes. (B) Pathway enrichment analysis of downregulated genes (n = 3).

somehow lead to less colony formation than Au nanoparticles and physically mixed Ce6 and Au NPs.

Apart from an external radiation source, we also used ^{18}F-FDG and ^{68}Ga-DOTATATE as the internal radiation sources. Though usually radionuclides ^{18}F and ^{68}Ga are used for PET

https://doi.org/10.1021/acsomega.5c04914
ACS Omega 2026, 11, 439−448

imaging, the previous research indicated that they can somehow activate Ce6 and induce cell death.[15] The Ce6−Au NPs exhibited evident cell killing ability under ^{68}Ga exposure, resulting around 80% U87 cells killed under 50 kBq, which is not seen for Au NPs-, Ce6-, and Au+Ce6-treated groups (Figure 3C). The CCK-8 results in Figure 3D reveal that the combination of ^{18}F-FDG and Ce6, Au NPs, and Ce6−Au did not show evident cell toxicity within 48 h. By contrast, the colony formation results show that the pure Au NPs could lead to worse prefoliation performance of U87 cells when combined with 200 kBq of ^{18}F-FDG. The interaction of ^{18}F-FDG and Au−Ce6 even led to lethal damage to U87 cells, and no colony was formed within 2 weeks (Figure S4).

To explore the mechanism of enhanced radiotherapy for Ce6−Au NPs, we performed a comprehensive analysis of unique and shared differentially expressed genes between the X-ray-treated group and the X-ray + Ce6−Au-treated group. This analysis identified a total of 34332 expressed genes. Notably, the inclusion of Ce6−Au led to the upregulation of 102 genes and the downregulation of 152 genes compared to the X-ray-treated group. Based on the FPKM values of the differentially expressed genes, we categorized them into clusters exhibiting similar expression patterns and conducted hierarchical clustering (Figure S6A) and volcano plot analysis (Figure S6B). Our findings revealed that the Ce6−Au-treated group exhibited significant upregulation in gene pathways associated with the NOD-like receptor signaling pathway, chemokine signaling pathway, and cytokine−cytokine receptor interaction (Figure 4a). Conversely, gene pathways linked to the Hippo signaling pathway and TGF-β signaling pathway were markedly downregulated (Figure 4b). These signaling pathways play critical roles in modulating the tumor microenvironment and tumor immune system.[21−23]

Ultrasmall gold nanoparticles were synthesized via a simple reduction method, and PEG-SH was used as a shape-controlling agent. The thiol-PEG will first coordinate with gold precursors and in this way forms intermediates. Thus, the amount of thiol-PEG used is essential for achieving a gold product with controlled morphology.[24] When the added amount of PEG-SH was relatively less than the Au precursor, the as-synthesized Au NPs showed a diverse morphology with a majority of spherical particles and less rod-like and triangle shapes. When the molar ratio of PEG-SH to Au precursor was 0.8, the diameter of Au NPs decreased to around 2 nm. The decreased size also led to the disappearance of the characteristic UV−vis absorption peak of Au NPs at 526 nm. BSA was used to modify the surface of Au nanoparticles; the successful coating of BSA was confirmed by FT-IR spectra and ζ-potential results. The naked Au atoms on the surface can interact with the H atom in the aqueous solution and form a hydrodynamic layer, and the introduction of BSA can cover the bared Au atoms and lower the hydrodynamic diameter.[25] Considering the later modification process, we chose the Au-BSA(1000)-2 sample which has successful BSA coating and uniform morphology for conjugating with Ce6.

The CLSM images indicate that the Au−Ce6 nanoparticles can be successfully taken up by the U87 cells and HeLa cells and end up in the cytoplasm. As shown in Figure 1H, Ce6−Au has several light absorption peaks from 300 to 700 nm, indicating that it may respond to visible light and can transfer photon energy to electron−hole pairs which are toxic to tumor cells.[26] Moreover, the electron paramagnetic resonance (EPR) results in Figure S8 demonstrate that the presence of Au NPs can benefit electron separation after excitation of Ce6. The CCK-8 experiment reveals that Ce6−Au shows evident toxicity to U87 cells under 4 Gy X-rays and 50 kBq ^{68}Ga-DOTATATE, while the ones exposed to ^{18}F-FDG showed negligible cytotoxicity. The decay of ^{68}Ga can produce more Cherenkov photons than ^{18}F, which may play a role in the excitation of Ce6−Au NPs.[27] Colony formation assay indicated that Au NPs and Au−Ce6 nanoparticles possess long-term toxicity to U87 cells exposed to ^{18}F-FDG and HeLa cells exposed to X-rays. The less effective therapeutic results of HeLa cells may be due to the relatively less cell uptake of the Au NPs compared to U87 cells. The mRNA sequencing results indicated that the addition of Ce6−Au can influence some gene pathways relevant to the TME and cell immune response within U87 cells.

To study the radiation enhancement mechanism of Ce6−Au nanoparticles, we compared the cell toxicity of Ce6−Au nanoparticles and physically mixed Ce6 and Au NPs, namely, the Au NPs+Ce6 group. The Ce6−Au is more effective in tumor killing than the Au NPs+Ce6 group, and the latter one even does not show better performance than pure Ce6 and Au NPs. The results indicate that there is certain interaction between Au and Ce6 under radiation exposure, and the interaction is most likely due to the low-energetic electrons produced after exposing Au NPs to radiation.[9,10] The range of these low-energy electrons is limited; they could only reach the closely grafted Ce6 molecules, excite them, and generate electron−hole pairs, which would further induce the production of reactive oxygen species (ROS) that are lethal to tumor cells. Based on the obtained results, we hypothesize that the Ce6−Au NPs can achieve enhanced radiotherapy via three effects: (a) direct effects with the deposited radiation power; (b) ROS produced by water radiolysis; (c) the low-energy electrons can excite the Ce6 molecules and produce ROS, while the appearance of Au NPs can further help the electron transportation and thus increase the ROS production.

4. CONCLUSION

This work aims to fabricate a radiosensitive nanoplatform based on Ce6−Au conjugates. PEG plays a key role as the shape-controlling reagent during the formation process of Au NPs. The obtained Ce6−Au NPs can affect the growth process of both U87 and HeLa cells under X-ray, ^{18}F, and ^{68}Ga exposure. While the physically mixed Au NPs and Ce6 molecules show negligible influence on tumor growth. Once given to U87 cells, Ce6−Au can work on the signaling pathways related to the tumor microenvironment and tumor cell proliferation and thus increase the radiosensitivity of tumor cells. Our research proves that the combination of Au NPs and Ce6 can make better use of the low-energy electrons generated during ionizing radiation and produce more ROS to kill tumor cells. Nevertheless, more study is required to further prove the function mechanism of the Ce6−Au conjugates and to explore the therapeutic effects on Ce6−Au in vivo.

■ ASSOCIATED CONTENT

Supporting Information

The Supporting Information is available free of charge at https://pubs.acs.org/doi/10.1021/acsomega.5c04914.

DLS analysis, ζ-potential measurements, colony formation assay, RNA-seq analysis, and EPR analysis (PDF)

https://doi.org/10.1021/acsomega.5c04914
ACS Omega 2026, 11, 439−448

AUTHOR INFORMATION

Corresponding Author

Meiyun Wang − *Department of Radiology, Henan Provincial People's Hospital & The People's Hospital of Zhengzhou University, Zhengzhou 450003, China; Biomedical Research Institute, Henan Academy of Sciences, Zhengzhou 450008, China;* orcid.org/0000-0001-8779-6184; Email: mywang@zzu.edu.cn

Authors

Huanhuan Liu − *Department of Radiology, Henan Provincial People's Hospital & The People's Hospital of Zhengzhou University, Zhengzhou 450003, China;* orcid.org/0000-0003-0548-895X

Bing Xu − *Department of Radiation Science and Technology, Delft University of Technology, 2629 JB Delft, The Netherlands*

Lijuan Chen − *Department of Radiology, Henan Provincial People's Hospital & The People's Hospital of Zhengzhou University, Zhengzhou 450003, China*

Xiaochen Li − *Department of Nuclear Medicine, Henan Key Laboratory of Novel Molecular Probes and Clinical Translation in Nuclear Medicine, Henan Provincial People's Hospital & The People's Hospital of Zhengzhou University, Zhengzhou 450003, China;* orcid.org/0000-0002-3215-1095

Huiqiang Li − *Department of Nuclear Medicine, Henan Key Laboratory of Novel Molecular Probes and Clinical Translation in Nuclear Medicine, Henan Provincial People's Hospital & The People's Hospital of Zhengzhou University, Zhengzhou 450003, China*

Junting Liang − *Clinical Bioinformatics Experimental Center, Henan Provincial People's Hospital, People's Hospital of Zhengzhou University, Zhengzhou 450003 Henan, China*

Yan Bai − *Department of Radiology, Henan Provincial People's Hospital & The People's Hospital of Zhengzhou University, Zhengzhou 450003, China*

Complete contact information is available at: https://pubs.acs.org/10.1021/acsomega.5c04914

Author Contributions

H. Liu carried out the majority of experiments and wrote the manuscript. B.X. carried out CLSM analysis. L.C. assisted with cell experiments. X.L. and H. Li were responsible for ^{18}F-FDG production and related radiation protection. J.L. performed mRNA sequencing analysis. Y.B. helped with manuscript writing. M.W. was involved in the experiment design and supervision.

Notes

The authors declare no competing financial interest.

ACKNOWLEDGMENTS

This study was financially supported by the National Key R&D Program of China (2023YFC2414200), National Natural Science Foundation of China General Program (82371934), Provincial Medical Science and Technology Research Joint Venture Project (LHGJ20240059 and LHGJ20240056), and Henan Provincial Science and Technology Research Program (252102310395 and 252102311208).

REFERENCES

(1) Wu, Y.; Song, Y.; Wang, R.; Wang, T. Molecular mechanisms of tumor resistance to radiotherapy. *Mol. Cancer* **2023**, *22*, 96.

(2) Zhang, H.; Zhao, H.; Chi, M.; Yang, K.; Chen, Y.; Mao, J.; Li, P.; Wang, Z.; Song, F.; Guo, W.; et al. A systematic review on the development of radiosensitizers, with cancer selectivity, for radiotherapy using ionizing radiation. *AIMS Bioeng.* **2023**, *10*, 89−110.

(3) Li, W. B.; Stangl, S.; Klapproth, A.; Shevtsov, M.; Hernandez, A.; Kimm, M. A.; Schuemann, J.; Qiu, R.; Michalke, B.; Bernal, M. A.; et al. Application of high-Z gold nanoparticles in targeted cancer radiotherapy-pharmacokinetic modeling, Monte Carlo Simulation and Radiobiological Effect Modeling. *Cancers* **2021**, *13*, 5370.

(4) Tarantino, S.; Capomolla, C.; Carla, A.; Giotta, L.; Cascione, M.; Ingrosso, C.; Scarpa, E.; Rizzello, L.; Caricato, A. P.; Rinaldi, R.; De Matteis, V. Shape-driven response of gold nanoparticles to X-rays. *Nanomaterials* **2023**, *13*, 2719.

(5) Wang, R.; Liu, H.; Antal, B.; Wolterbeek, H. T.; Denkova, A. G. Ultrasmall gold nanoparticles radiolabeled with Iodine-125 as potential new radiopharmaceutical. *ACS. Appl. Bio. Mater.* **2024**, *7*, 1240−1249.

(6) Petrik, N. G.; Alexandrov, A. B.; Vall, A. I. Interfacial Energy Transfer during Gamma Radiolysis of Water on the Surface of ZrO_2 and Some Other Oxides. *J. Phys. Chem. B* **2001**, *105*, 5935−5944.

(7) Sharmah, A.; Yao, Z.; Lu, L.; Guo, T. X-ray-induced energy transfer between nanomaterials under X-ray irradiation. *J. Phys. Chem. C* **2016**, *120*, 3054−3060.

(8) Xiong, Z.; Yang, M.; Liu, P.; Tang, Z.; Yang, Y.; Zhan, M.; Chen, T.; Li, X.; Lu, L. Designing bimetallic Metal-Organic Framework-based heterojunction radiosensitizer for enhanced radiodynamic therapy and immunotherapy. *Adv. Funct. Mater.* **2023**, *34*, No. 2312919.

(9) Wang, X.; Zhang, C.; Du, J.; Dong, X.; Jian, S.; Yan, L.; Gu, Z.; Zhao, Y. Enhanced generation of non-oxygen dependent free radicals by Schottky-type heterostructures of Au-Bi$_{(2)}$S$_{(3)}$ nanoparticles via X-ray-Induced catalytic reaction for radiosensitization. *ACS Nano* **2019**, *13*, 5947−5958.

(10) Cheng, K.; Sano, M.; Jenkins, C. H.; Zhang, G.; Vernekohl, D.; Zhao, W.; Wei, C.; Zhang, Y.; Zhang, Z.; Liu, Y.; et al. Synergistically enhancing the therapeutic effect of radiation therapy with radiation activatable and reactive oxygen species-releasing nanostructures. *ACS Nano* **2019**, *13*, 5947−5958.

(11) Koczorowski, T.; Glowacka-Sobotta, A.; Michalak, M.; Mlynarczyk, D. T.; Güzel, E.; Goslinski, T.; Sobotta, L. Connections between metallic nanoparticles and Chlorin e6—An overview of physicochemical and biological properties and prospective medical applications. *Appl. Sci.* **2023**, *13*, 3933.

(12) Zhang, H.; Li, H.; Fan, H.; Yan, J.; Meng, D.; Hou, S.; Ji, Y.; Wu, X. Formation of plasmon quenching dips greatly enhances $^1O_2$ generation in a chlorin e6−gold nanorod coupled system. *Nano Res.* **2018**, *11*, 1456−1469.

(13) Liu, H.; Laan, A. C.; Plomp, J.; Parnell, S. R.; Men, Y.; Dalgliesh, R. M.; Eelkema, R.; Denkova, A. G. Ionizing radiation-induced release from Poly(ϵ-caprolactone-b-ethylene glycol) micelles. *ACS Appl. Polym. Mater.* **2021**, *3*, 968−975.

(14) Tu, Z.; Sang, Z.; Xu, Y.; Liang, W.; Qiao, S.; Sun, Q.; Feng, K.; Kong, Z.; Wang, H.; Liu, Z. Porphyrin-engineered ^{125}I-nanoseeds as a prototype for immunogenic brachytherapy. *J. Am. Chem. Soc.* **2025**, *147*, 13229−13242.

(15) Kamkaew, A.; Cheng, L.; Goel, S.; Valdovinos, H. F.; Barnhart, T. E.; Liu, Z.; Cai, W. Cerenkov radiation induced photodynamic therapy using Chlorin e6-loaded hollow mesoporous silica nanoparticles. *ACS Appl. Mater. Interfaces* **2016**, *8*, 26630−26637.

(16) Leopold, L. F.; Tódor, I. S.; Diaconeasa, Z.; Ruginǎ, D.; Ştefancu, A.; Leopold, N.; Coman, C. Assessment of PEG and BSA-PEG gold nanoparticles cellular interaction. *Colloids Surf., A* **2017**, *532*, 70−76.

(17) Mochizuki, C.; Nakamura, J.; Nakamura, M. Effects of Au States in Thiol-organosilica nanoparticles on enzyme-like activity for X-ray sensitizer application: focus on reactive oxygen species generation in radiotherapy. *ACS Omega* **2023**, *8*, 9569−9582.

(18) Sharma, V.; Javed, B.; Estrada, G.; Byrne, H. J.; Tian, F. In situ tuning and investigating the growth process of size controllable gold

nanoparticles and statistical size prediction analysis. *Colloids Surf., A* **2024**, *681*, No. 132733.
(19) Piella, J.; Bastus, N. G.; Puntes, V. Size-dependent protein-nanoparticle interactions in citrate-stabilized gold nanoparticles: the emergence of the protein corona. *Bioconjugate Chem.* **2017**, *28*, 88−97.
(20) Jiang, F.; Yang, C.; Ding, B.; Liang, S.; Zhao, Y.; Cheng, Z.; Liu, M.; Xing, B.; Ma, Pa.; Lin, J. Tumor microenvironment-responsive $MnSiO_3$-Pt@BSA-Ce6 nanoplatform for synergistic catalysis-enhanced sonodynamic and chemodynamic cancer therapy. *Chin. Chem. Lett.* **2022**, *33*, 2959−2964.
(21) Quail, D. F.; Joyce, J. A. The Microenvironmental landscape of brain tumors. *Cancer Cell* **2017**, *31*, 326−341.
(22) Kim, E. H.; Sohn, B. H.; Eun, Y. G.; Lee, D. J.; Yim, S. Y.; Kang, S. G.; Lee, J. S. Silence of hippo pathway associates with pro-tumoral immunosuppression: potential therapeutic target of glioblastomas. *Cells* **2020**, *9*, 1761.
(23) Tschernia, N. P.; Gulley, J. L. Tumor in the Crossfire: Inhibiting TGF-beta to Enhance Cancer Immunotherapy. *BioDrugs* **2022**, *36*, 153−180.
(24) Liu, J.; Yu, M.; Ning, X.; Zhou, C.; Yang, S.; Zheng, J. PEGylation and zwitterionization: pros and cons in the renal clearance and tumor targeting of near-IR-emitting gold nanoparticles. *Angew. Chem., Int. Ed.* **2013**, *52*, 12572−12576.
(25) Bolanos, K.; Kogan, M. J.; Araya, E. Capping gold nanoparticles with albumin to improve their biomedical properties. *Int. J. Nanomed.* **2019**, *14*, 6387−6406.
(26) Ma, T.; Zhang, Q.; Xuan, Q.; Zhuang, J.; Zhang, W.; Li, H.; Chen, C.; Wang, P. pH/near-infrared light dual activated Ce6-doped silicon nanoparticles with tumor chemo-photodynamic synergistic therapy for improving efficiency of monotherapy. *J. Chem. Eng.* **2021**, *424*, No. 130536.
(27) Duan, D.; Liu, H.; Xu, Y.; Han, Y.; Xu, M.; Liu, Z. Activating TiO_2 nanoparticle: Gallium-68 serves as a high-yielded photon emitter for Cerenkov induced photodynamic therapy. *ACS Appl. Mater. Interfaces* **2018**, *10* (6), 5278−5286.

https://doi.org/10.1021/acsomega.5c04914
ACS Omega 2026, 11, 439−448